Generation of an ordered Ge quantum dot array in an amorphous silica matrix by ion beam irradiation: Modeling and structural characterization

M. Buljan,[1,2] I. Bogdanović-Radović,[2] M. Karlušić,[2] U. V. Desnica,[2] N. Radić,[2] N. Skukan,[2] G. Dražić,[3] M. Ivanda,[2] O. Gamulin,[4] Z. Matej,[1] V. Valeš,[1] J. Grenzer,[5] T. W. Cornelius,[6] H. T. Metzger,[6] and V. Holý[1]

[1]*Charles University in Prague, Ke Karlovu 5, 12160 Prague, Czech Republic*

[2]*Ruđer Bošković Institute, Bijenička cesta 54, 1000 Zagreb, Croatia*

[3]*Jožef Stefan Institute, Jamova 39, 1000 Ljubljana, Slovenia*

[4]*University of Zagreb, School of Medicine, Šalata 3, 10000 Zagreb, Croatia*

[5]*Forschungszentrum Dresden-Rossendorf, P.O. Box 510119, 01314 Dresden, Germany*

[6]*European Synchrotron Radiation Facility (ESRF), BP 220, F-38043 Grenoble, France*

(Received 13 November 2009; revised manuscript received 21 December 2009; published 17 February 2010)

We studied the generation of an ordered Ge quantum dot array in an amorphous silica matrix by ion beam irradiation. In particular we investigated the influence of the irradiation process on the nucleation of Ge clusters, on the correlations in their positions and on the crystalline quality of Ge quantum dots formed after subsequent annealing. We have developed a method for the description of the intensity of grazing-incidence x-ray small-angle scattering from irradiated multilayers, which enables a precise determination of the arrangement of quantum dots as well as their position correlation and size distribution. The analysis shows that the irradiation causes an ordering of Ge clusters along the irradiation direction, which substantially improves the correlations of the Ge dot locations in their three-dimensional array. The observed phenomena are explained and simulated by a Monte Carlo model based on the modification of local Ge density induced by ion tracks in the irradiated multilayers.

DOI: 10.1103/PhysRevB.81.085321 PACS number(s): 81.07.Ta, 81.07.Bc, 68.65.−k

I. INTRODUCTION

Semiconductor quantum dots (QDs) are intensively investigated in the last decade due to their unique and size-tunable properties which enable wide range of their applications.[1–6] The electronic and optical properties of QDs are determined mostly not only by their composition and size, but also by their inner structure and crystalline quality. The arrangement of QDs in the matrix is also very important since it affects the macroscopic properties of a dot-containing composite material. The regular arrangement of QDs can induce their collective vibrations[7–9] or an appearance of minibands of eigenenergies due to overlapping of the wave functions of electrons confined in QDs.[10] Moreover, the regularity of the QD arrangement narrows the size distribution of the dots,[9] which is a very important factor for technological applications. Therefore, a precise control of the QD size, the inner structure, and the QD arrangement in the matrix is an important issue.

Germanium QDs embedded in an amorphous SiO_2 matrix show very strong quantum confinement effects,[11,12] electroluminescence and photoluminescence,[13,14] nonlinear properties,[15] unusual melting-freezing conditions,[16] and a possibility to store electric charge for a long time.[17,18] Therefore, they have a lot of potential applications in the production of QD based memory devices, solar cells, and numerous other optoelectronic devices.

In our recent research[19] we have shown a possibility of production of well-ordered three-dimensional (3D) lattices of Ge QDs in amorphous SiO_2, where a long-range type of ordering is achieved within the whole volume of the investigated material. The ordering is induced by an irradiation of amorphous $(Ge+SiO_2)/SiO_2$ multilayers by oxygen ions, which causes a nucleation of Ge QDs along the direction of the tracks of the irradiating ions. A subsequent annealing after the irradiation process induces a crystallization of QDs and an appearance of a distinct well-ordered 3D lattice of Ge QDs in the amorphous SiO_2 matrix.

Here, we investigate in detail the structural properties of the QD lattices formed by the above mentioned procedure and effects of an ion beam irradiation on the spatial arrangement, size, and size distribution, as well as on the crystalline quality of the formed QDs. We apply a combination of different experimental methods, namely, transmission electron microscopy (TEM), high-resolution transmission electron microscopy, and grazing-incidence small-angle x-ray scattering (GISAXS) for the investigation of the dot arrangement and sizes, while x-ray diffraction (XRD) and Raman and infrared (IR) spectroscopy are used for the study of the inner structure of QDs and of the surrounding matrix. We develop a model for the analysis of GISAXS intensity maps measured on the irradiated samples, which allows us to determine the basis vectors of the 3D lattice of the QDs, the statistical deviations of the QD positions from the ideal positions, the sizes of the QDs, and the size distribution. A model for Monte Carlo simulation of the positions of QDs is developed as well.

The results of the applied analysis demonstrate the formation of Ge-density fluctuations in the Ge-rich layers of the $(Ge+SiO_2)/SiO_2$ multilayer system, caused by the irradiation. The formed fluctuations are spatially correlated in the irradiation direction as well as in the plane parallel to the substrate, and they transform to a 3D lattice of spherical and crystalline Ge QDs during the subsequent annealing. The observed phenomena are explained and modeled successfully by a simple phenomenological Monte Carlo approach

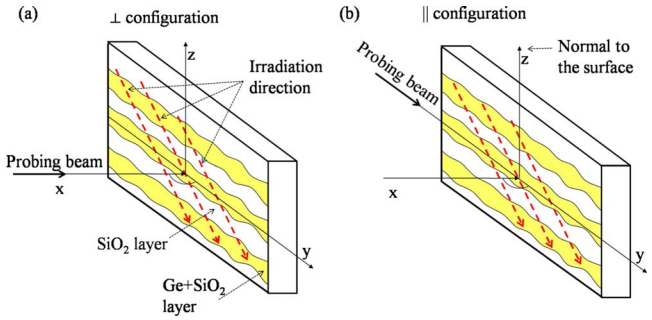

FIG. 1. (Color online) Geometries used for the GISAXS and TEM measurements. The irradiation direction is indicated by the dashed arrows. The probing beam is (a) perpendicular ($\perp$) and (b) parallel ($\parallel$) to the irradiation plane.

based on the modification of the local density of Ge atoms induced by the energy deposition from the ions used for irradiation. The analysis of the crystalline quality of the QDs, which are formed in the irradiated multilayers during annealing, demonstrates that their inner structure is the same or even better than in the nonirradiated samples. A good degree of ordering and good crystalline quality of the formed QDs indicate that this relatively simple method has a potential for the production of photonic crystals or photovoltaic devices.

The paper is organized as follows. In Sec. II we present details of the deposition and measurement procedures. The arrangement and the size properties of the QDs, as well as the method used for the analysis of the GISAXS intensity distributions are investigated in Sec. III. In Sec. IV, we develop a Monte Carlo model explaining the observed arrangement of QDs. The crystalline quality and inner structure of QDs and of the surrounding matrix are investigated in Sec. V, and conclusions are drawn in Sec. VI.

II. EXPERIMENTAL PROCEDURE

Twenty $(Ge+SiO_2)/SiO_2$ bilayers were deposited onto Si(111) substrate by magnetron sputtering codeposition. The deposition was performed at room temperature, with the molar ratio of $Ge:SiO_2$ of 60:40 in the mixed layers. The mixed layers were separated by layers of pure SiO_2. The nominal period was 15 nm; the thickness ratio of $(Ge+SiO_2):SiO_2=1:1$. After the deposition, the resulting multilayers were irradiated with 3 MeV $^{16}O^{3+}$ ions with a fluence of 1×10^{15} ions cm^{-2}, under the angle $\varphi_{irr}=60°$ with respect to the surface. The energy of the oxygen ions was high enough to ensure approximately straight trajectories of ions through the multilayer and their stopping deeply in the Si substrate (the approximate projected range is 2.5 μm). In this way, the ion beam interacts with the multilayer only by energy transfer, not changing the atomic composition of the multilayer. After the irradiation, both irradiated and nonirradiated multilayers were annealed in vacuum at 800 °C for 1 h, with a temperature ramp of 10 °C/min. The ramp was slightly smaller then in Ref. 19, where a formation of larger clusters was observed in the surface layer. This decreased rate resulted in a smooth surface and a more homogeneous distribution of the material through the multilayer. Raman

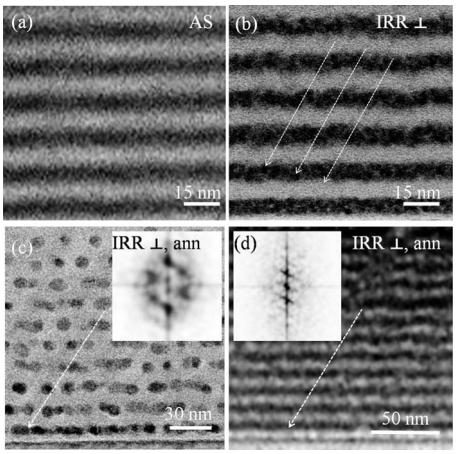

FIG. 2. TEM cross sections of the (a) as-deposited and (b) irradiated multilayers before annealing taken in the $\perp$ direction. (c) and (d) TEM cross sections in the $\perp$ direction of the irradiated multilayer after annealing obtained with two different magnifications. The insets show the Fourier transformations of the corresponding TEM images.

scattering experiments were carried out at room temperature by using the subtractive configuration of a Jobin Yvon T64000 triple monochromator. The spectral resolution was 0.5 cm^{-1}. The 514.5 nm laser excitation beam of an Ar-ion laser was focused to the diameter of 40 μm and the laser power on the sample was 70 mW. Transmission electron microscopy images have been taken at the JEOL2010F microscope, operated at 200 kV, and equipped with a field-emission gun and a high-angle annular dark-field detector (HAADF) for *Z*-contrast imaging. GISAXS measurements were performed at European Synchrotron Radiation Facility (ESRF) Grenoble, France, ID01 beamline. Two-dimensional (2D) GISAXS intensity maps were measured using a one-dimensional position-sensitive detector (PSD) mounted perpendicularly to the sample surface; the 2D maps were collected by moving the PSD along the sample surface. An incident x-ray radiation with a wavelength of 0.1127 nm was used, while the incidence angle was set slightly above the critical angle of total reflection. The chosen incidence angle enabled us to study the whole thickness of the investigated multilayers. XRD measurements were taken in grazing-incidence geometry with an incidence angle of 0.3°, using Cu $K\alpha$ radiation and a standard laboratory diffractometer equipped with a parabolic multilayer optics and a secondary graphite monochromator. In order to asses the structural anisotropy induced by the irradiation, we have used two geometries for GISAXS and TEM measurements, shown in Fig. 1, in which the probing beam is perpendicular or parallel to the irradiation plane (defined by the ion beam direction and sample surface normal).

III. ANALYSIS OF THE FORMATION, SIZE, AND ARRANGEMENT OF QUANTUM DOTS

Figure 2 shows the TEM micrographs of the multilayers before and after the irradiation. In the former case, Ge and SiO_2 are homogeneously mixed in the Ge-rich layers, with

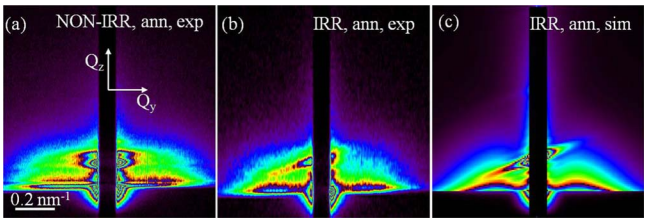

FIG. 3. (Color online) GISAXS maps of the annealed multilayers: (a) nonirradiated and (b) irradiated taken in the ⊥ configuration; (c) simulation of the map of the irradiated multilayer. $Q_{y,z}$ are the scattering vectors in the detector plane.

no visible clustering of Ge atoms, as can be seen in Fig. 2(a). However, in the cross section of the irradiated multilayer, shown in Fig. 2(b), fluctuations in Ge density (or clustering of Ge atoms) are clearly visible. High-resolution TEM measurements of the same sample (not shown here) show that formed clusters are mainly amorphous and they are not separated by pure SiO_2 matrix but with $Ge+SiO_2$ mixture with a lower Ge content. In the same TEM image, the ordering of the formed clusters along the irradiation direction is indicated. Thus, we can conclude that the ions used for the irradiation cause clustering of Ge atoms and consequently trigger their ordering in the irradiation direction. Very similar results showing ordering of QDs along the lines in the irradiation direction are observed at different irradiation angles φ_{irr} in the range from 45° to 60° (not shown here). The TEM cross sections of the irradiated multilayer after annealing are presented in Figs. 2(c) and 2(d) where separate nearly spherical clusters are visible, ordered along the irradiation direction as well. The ordering of the QDs along the irradiation direction also follows from the Fourier transformations of the TEM images shown in the insets of Figs. 2(c) and 2(d). From this findings it follows that the annealing causes a transformation of Ge-density fluctuation into well separated Ge QDs.

The GISAXS intensity distributions of the nonirradiated and irradiated multilayers after annealing are shown in Figs. 3(a) and 3(b), respectively. For the nonirradiated multilayer, the intensity distribution was not sensitive to the azimuthal orientation of the sample with respect to the probing x-ray beam, indicating a homogeneous and isotropic distribution of QDs in the plane parallel to the multilayer surface. The irradiated multilayer exhibits a completely different pattern, namely, the ordering of QDs gives rise to of tilted Bragg sheets[20] that are perpendicular to the direction of irradiation.

Thus, the experimentally measured Bragg sheets represent a cross section of the three-dimensional sheetlike intensity distribution in reciprocal space with the Ewald sphere (represented roughly by a vertical plane nearly perpendicular to the primary beam) being tilted for all azimuthal orientations of the samples, except for the ∥ orientation, where the observed sheets are horizontal. The tilt angle (measured with respect to the horizontal Q_y axis) of the sheets changes continuously from zero (in the ∥ configuration) to $\pi/2-\varphi_{\mathrm{irr}}$ obtained for the ⊥ configuration, which is shown in Fig. 3(b). The GISAXS intensity maps obtained from the nonirradiated and from the irradiated multilayers in the ∥ configuration are shown in our previous paper.[19]

For a more precise analysis of the GISAXS intensity maps we have developed a model based on the well-known

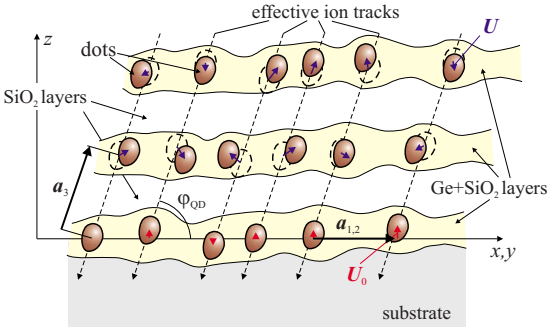

FIG. 4. (Color online) Schematic sketch of the 3D paracrystal model used for the analysis of the GISAXS data.

paracrystal dot arrangement.[21] In addition to the standard paracrystal model we have assumed that the total intensity is given by a superposition of the quantum dot and interface roughness contributions. We assumed that the dots have the form of uniaxial ellipsoids with lateral and vertical radii R_L and R_V, respectively, and the random dot sizes are distributed according to the gamma distribution with the root-mean-square (rms) deviation σ_R.

The model assumes that the average lattice of QDs is described by three basis vectors $\boldsymbol{a}_{1,2,3}$. The first two vectors lie in the plane parallel to the substrate and generate a 2D hexagonal paracrystal array (the angle between $\boldsymbol{a}_1$ and $\boldsymbol{a}_2$ generally can be different from 60°), while the third basis vector $\boldsymbol{a}_3$ is along the ordering of the dots at subsequent interfaces and it makes an angle φ_{QD} with the sample surface (see Fig. 4). In the case of ideal ordering of the QDs along the irradiation direction, the angle φ_{QD} equals the irradiation angle φ_{irr}. Thus, the type of the formed three-dimensional QD lattice depends on the irradiation angle; a simple hexagonal lattice is expected for the normal incidence of the irradiating ions ($\varphi_{\mathrm{irr}}=90°$), while the irradiation under $\varphi_{\mathrm{irr}}=60°$ leads to a fcc-like or a hcp-like lattice. However, in contrast to the weaker dot self-organization in nonirradiated multilayers reported previously in Ref. 8, the fcc-like dot ordering in an irradiated multilayer is not an "intrinsic" property of the ordering mechanism since any other irradiation angle gives rise to a three-dimensional dot lattice without the threefold (or sixfold) vertical symmetry axis.

The 2D hexagonal in-plane ordering is based on the results of the analysis of the experimentally measured GISAXS spectra for various azimuthal orientations with respect to the probing beam direction. For the irradiation angles close to the normal incidence angle, the analysis shows the formation of approximately uniformly spaced and uniformly distributed QDs in the planes parallel to the substrate. Therefore, the 2D hexagonal paracrystal is an excellent approach for such a kind of ordering. However, for the irradiation angles which are not close to the normal incidence angle, the 2D hexagonal array may be distorted, i.e., elongated in the irradiation direction. For that case an angle between the basis vectors $\boldsymbol{a}_1$ and $\boldsymbol{a}_2$ is different from 60°.

The in-plane deviations of the positions of QDs from the ideal hexagonal lattice determined by integer linear combinations of the average lattice vectors $\boldsymbol{a}_{1,2}$ are described by a short-range order model with the rms deviation σ_{LL}. This

TABLE I. Structural parameters of the nonirradiated (nonirr.) and irradiated (irr.) multilayers determined from the GISAXS data. The first seven parameters define the lattice of QDs. a_{3z} denotes the z component of the basis vector $\boldsymbol{a}_3$, $R_{L,V}$ are the mean lateral and vertical radii of the dots, σ_R is their rms dispersion, σ is rms interface roughness, and c_{Ge} is the Ge concentration of $\mathrm{Ge}+\mathrm{SiO_2}$ mixture between Ge QDs normalized to unity. Since the nonirradiated and non-annealed multilayers do not exhibit any clustering of Ge atoms, the parameters of the quantum dot model are missing in the corresponding data column.

Parameters	Nonirr.	Irr.	Nonirr. ann.	Irr. ann.
φ_{QD} (deg)	90 ± 0	65 ± 2	90 ± 0	65 ± 2
$\lvert\boldsymbol{a}_{1,2}\rvert$ (nm)		20 ± 2	14.5 ± 0.6	21.6 ± 0.4
$\lvert\boldsymbol{a}_{3z}\rvert$ (nm)		14.8 ± 0.2	14.8 ± 0.2	14.8 ± 0.2
σ_{LL} (nm)		4 ± 2	5.4 ± 0.8	4.2 ± 0.4
σ_{VL} (nm)		4 ± 1	8.1 ± 0.6	4.2 ± 0.4
σ_{LV} (nm)		0.1 ± 0.1	0.2 ± 0.1	0.2 ± 0.1
σ_{VV} (nm)		0.3 ± 0.1	0.2 ± 0.1	0.2 ± 0.1
R_L (nm)		3.6 ± 0.6	3.2 ± 0.2	4.1 ± 0.1
R_V (nm)		3.2 ± 0.5	3.2 ± 0.3	3.9 ± 0.2
σ_R (nm)		1.1 ± 0.4	1.0 ± 0.6	0.7 ± 0.1
σ (nm)	2.1 ± 0.2	2.5 ± 0.2	2.4 ± 0.4	2.4 ± 0.5
c_{Ge}	0.6 ± 0.1	0.24 ± 0.08	0.10 ± 0.06	0.07 ± 0.06

parameter describes the random deviations in the lateral distances of the neighboring dots lying at first (substrate) interface. The vertical deviations $\boldsymbol{U}_0$ of these dots from the mean substrate surface are described by long-range order model with the rms deviation σ_{LV}. From the actual positions of the dots at the first interface the mean positions of the dots at subsequent interfaces are derived; these positions are denoted by dashed lines in Fig. 4. The random deviations $\boldsymbol{U}$ of the dots from these mean positions at interfaces $2,\ldots,N$ are characterized by two rms deviations: σ_{VL} and σ_{VV}; the former accounts for the random lateral displacements from ion tracks, while the latter describes the vertical displacements, i.e., the random local deviations from the mean multilayer period (long-range order). The details of the model as well as the formulas for the scattered intensity are given in the Appendix.

We have analyzed the GISAXS maps measured on the nonirradiated and irradiated multilayers after annealing. The experimental data are shown in Fig. 3. The data for the nonannealed multilayers have been presented already in our previous work in Ref. 19. The parameters obtained by the fitting of all maps are summarized in Table I. In the discussion of the results, we start with the comparison of the GISAXS results obtained on the nonirradiated and irradiated multilayers after annealing; the corresponding GISAXS maps are shown in Figs. 3(a) and 3(b). The comparison of these maps shows that a better degree of the dot ordering is achieved in the irradiated sample, both in the irradiation and in the lateral directions. The difference in the measured value of the correlation angle of the QDs ($\phi_{QD}=65°$) from the nominal irradiation angle ($\varphi_{\mathrm{irr}}=60°$) is smaller than the uncertainty limits of the determination of both angles. A vertical (interplane) correlation in the QD positions exists also in the nonirradiated samples, however, with the degree of correlation being much smaller. This conclusion follows from the higher contribution of the interface roughness and higher value of the disorder parameter (σ_{LV}) for the nonirradiated sample.

The correlation of the dot positions within the individual 2D dot arrays (i.e., the lateral correlation of the dot positions) gives rise to lateral satellite peaks in the GISAXS maps, visible only in the irradiated samples [Figs. 3(b) and 3(c)]. Therefore, the lateral ordering of QDs is much better in the irradiated samples, i.e., the in-plane deviation (σ_{LL}) describing the disorder of the in-plane distances of QDs ($\langle\lvert\boldsymbol{a}_{1,2}\rvert\rangle$) is much smaller. A detailed analysis of the nonirradiated samples is presented in Ref. 22 showing a formation of QDs within Ge-rich layers, but the positions of the formed dots are not correlated. A better spatial correlation of the positions of QDs also affects their size distribution; the rms deviation of the QD sizes σ_R is smaller in the irradiated multilayer.

Let us summarize all results obtained by the TEM and GISAXS analyses. In the as-deposited nonirradiated multilayers the layers are homogeneous without a pronounced cluster formation. The TEM cross sections show practically no Ge clustering, while GISAXS results demonstrate a dominant contribution of the interface roughness to the GISAXS intensity. During the annealing of the nonirradiated samples, quantum dots are formed in the Ge-rich layers, but the correlation of their positions is very weak.

In contrary, the irradiation of the multilayers leads to Ge-density fluctuations in Ge-rich layers already before annealing, so that both the interface roughness and Ge clusters contribute to the GISAXS intensity. During annealing, the maxima of the fluctuations of the Ge density transform to well-separated and spherical crystalline Ge QDs and they retain their initial arrangement (the in-plane separation of the QDs, $\lvert\boldsymbol{a}_{1,2}\rvert=20\pm2$ nm, has the same values as before annealing). Thus, after annealing we obtain a lattice of well-ordered Ge QDs in the $\mathrm{SiO_2}$ matrix. The in-plane separation of the Ge clusters (or the QDs after annealing) is larger in the irradiated multilayers than in the nonirradiated ones, in which $\lvert\boldsymbol{a}_{1,2}\rvert=14.5\pm0.6$ nm; the size of the clusters (or QDs) increases with the irradiation as well. The shape of the QDs is close to spherical ones; however, the most regular shape shows the irradiated samples after annealing. The multilayer period is the same for all multilayers, $a_{3z}=14.8\pm0.2$ nm. The rms roughness of the interfaces between the $\mathrm{SiO_2}$ and $\mathrm{SiO_2}+\mathrm{Ge}$ layers was about 2 nm for both nonirradiated and irradiated samples. Since the density c_{Ge} of Ge atoms in the $\mathrm{SiO_2}+\mathrm{Ge}$ layers between the dots substantially decreases during the annealing, the contrast of the refraction indices of the $\mathrm{SiO_2}$ spacer layers and the $\mathrm{SiO_2}+\mathrm{Ge}$ layers is very weak, so that the GISAXS maps of the annealed samples are almost not sensitive to the interface roughness.

In order to determine a possible loss of Ge atoms from the Ge-rich layers and from the Ge QDs due to the irradiation and/or annealing, we calculated the Ge concentration $\langle c_{\mathrm{Ge}}\rangle$ as an average of the concentration c_{Ge} in the Ge-rich layers between the QDs and the Ge concentration in the QDs (assumed unity). In addition to the c_{Ge} values we used the mean dot distances $\lvert\boldsymbol{a}_{1,2}\rvert$ and the dot radii $R_{L,V}$ for this cal-

culation; the numerical values of these parameters are listed in Table I. For the nonirradiated and irradiated samples we obtained $\langle c_{\mathrm{Ge}} \rangle = 0.60 \pm 0.05$ and $\langle c_{\mathrm{Ge}} \rangle = 0.57 \pm 0.03$, respectively. These densities agree very well with the nominal value of 0.6, following from the nominal molar ratio $\mathrm{Ge}:\mathrm{SiO_2} = 60:40$ during the deposition. This fact demonstrates that there are practically no Ge losses during the annealing, and the influence of the irradiation on the Ge loss is negligibly small.

IV. MODEL OF THE NUCLEATION AND GROWTH OF QUANTUM DOTS

In this section we present a simple phenomenological model explaining the experimentally observed chain-line nucleation and growth of quantum dots along the ion tracks. The model is based on the fact that the mean lateral distance $|\boldsymbol{a}_{1,2}|$ between the QDs of approximately 20 nm is much larger than the average distance between two neighboring ion trajectories in the multilayer ($L_{\mathrm{ion}} \approx 0.15$ nm). Thus, the formation of the Ge-density fluctuation resulting in the dot formation is not a consequence of a single ion transmission through the multilayer like in Ref. 23; it can be explained rather by the energy deposition in the multilayer by the irradiation process.[24,25]

Passing through the material, the ion deposits energy to the neighboring material along its trajectory.[23,26] The calculated electronic stopping power for the ions used for irradiation is 1.8 keV/nm,[27] in SiO_2 matrix, and the typical radius of the cylindrical region around an ion trajectory where 65% of its energy is deposited is estimated in the range of about 1–5 nm.[28] The deposited energy acts in a similar way as thermal annealing, i.e., it facilitates the diffusion of deposited Ge atoms into the cylindrical region, and their agglomeration.[25]

We propose a simple model for a qualitative description of the observed ordering of the positions of the QDs, which is presented in Fig. 5. We assume that the multilayer with an initially constant Ge density in the Ge-rich layers is irradiated with ions under the angle $\varphi_{\mathrm{irr}} = 60°$ with respect to the sample surface. The ions pass through the multilayer along straight trajectories, which are parallel but randomly chosen with a uniform distribution of their lateral coordinates. The model further assumes a diffusion of Ge atoms in the Ge-rich layers toward the centers of the ion beam tracks, which are formed by the ions passing through material. This model is supported by the fact that the amount of deposited energy is the highest in the center of the tracks[24,28] and that the energy deposited by the ion causes formation of small Ge clusters (Ge nuclei) via diffusion mechanism.[29] In this way, the Ge density is increased in the center of the track, while a depleted region forms at the track outskirts. A simplified profile of the density of the Ge atoms after irradiation of the multilayer with a single ion, assuming an initially constant Ge density, is shown in Fig. 5(a); its form is chosen in agreement with the nuclei formation mechanism and the well-known Ham theory of diffusion-driven precipitation.[30] The rms deviation of the Gaussian-like profile of Ge density across a single track was set to 4.5 nm, in agreement with the finding in Ref. 28, taking into account the irradiation angle. Within this simplified model, each incoming ion changes the local Ge density in the small region within its track. The resulting 2D distribution of the Ge density is therefore a convolution of the density profile around a single track [shown in Fig. 5(a)] with a randomly fluctuating local density of incoming ions.

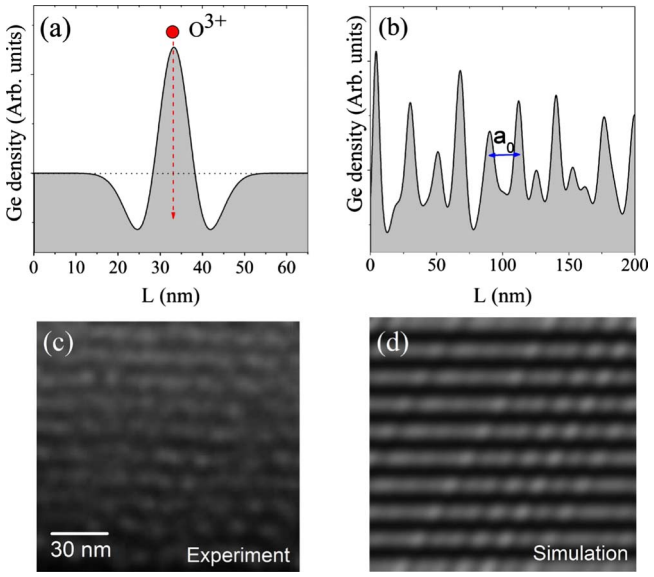

FIG. 5. (Color online) (a) The simplified lateral profile of the density of Ge atoms in the $Ge+SiO_2$ layer around a single ion track used for the numerical simulation of the nucleation. A constant Ge density assumed before the irradiation is denoted by the dotted line; L is the coordinate parallel to the layer surface. (b) The simulated profile of the Ge density in the same layer after the irradiation with the fluence of 1×10^{15} ions/cm^2. (c) TEM cross section of the annealed multilayer. (d) The simulated Ge density obtained assuming a formation of spherical Ge QDs during annealing.

We have performed a series of numerical simulations which show that, after the irradiation by many ions, fluctuations of the Ge density appear with the average distance of ≈ 20 nm [Fig. 5(b)]. This distance depends on the track diameter and on the diameter of the Ge-depleted region around the ion track. This finding is in a good agreement with the measured data ($|\boldsymbol{a}_{1,2}| = 20 \pm 2$ nm). Thus, the distance between the QDs is determined mostly by the width of the interaction profile, less by the average distance between neighboring tracks. The formed fluctuations are spatially correlated along the direction of the ion beam and they act as nucleation centers for the growth of crystalline quantum dots during a subsequent annealing. The experimentally measured TEM image and the simulation of the Ge density after annealing are shown in Figs. 5(c) and 5(d), respectively. A more detailed study of the nucleation process including experimental measurements of the ion track widths will be the topic of our future work.

V. INFLUENCE OF IRRADIATION ON THE ATOMIC STRUCTURE OF THE QDs AND THE SURROUNDING MATRIX

It is well known that irradiation process can damage the irradiated material. In this section we explore the influence

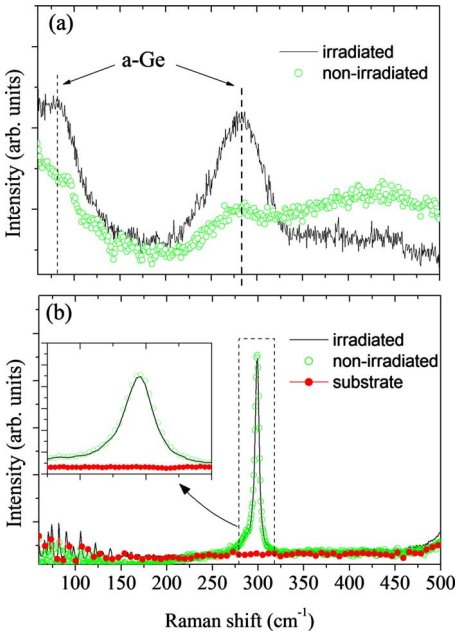

FIG. 6. (Color online) Raman spectra of the irradiated and nonirradiated multilayers (a) before and (b) after annealing. In the spectra measured before annealing, amorphous Ge bands close to 80 and 275 cm^{-1} (denoted by a-Ge and dashed lines) are visible. The inset in (b) shows the enlarged TO Ge peak at 300 cm^{-1}.

of the irradiation on the internal atomic structure and on the crystalline quality of the QDs formed after annealing of the irradiated multilayers, and the effect of the irradiation on the amorphous SiO_2 matrix.

Figure 6 shows the Raman spectra of the irradiated and nonirradiated samples before and after annealing process. Before annealing [Fig. 6(a)], two broad Ge bands centered close to 80 and 275 cm^{-1} are visible in the both spectra. The bands show the existence of amorphous Ge both in irradiated and nonirradiated multilayers. However, the bands are much more pronounced in the irradiated multilayers; this is in agreement with the formation of amorphous Ge clusters by the irradiation procedure. After annealing [Fig. 6(b)], both spectra exhibit a very sharp Ge TO peak at 300 cm^{-1} and have similar shapes and widths [see the inset in Fig. 6(b)]. This result reveals a very weak influence of the irradiation on the internal structure of the QDs formed after annealing. Moreover, the Si-Ge vibrations usually appearing between 310 and 500 cm^{-1} are absent in both spectra. The width of the TO peak of the irradiated multilayer is slightly narrower (confirmed by the fit of the peak widths), in agreement with the formation of larger QDs in that sample. The small difference in the widths of the TO peaks is the consequence of different size distributions of the dots in the irradiated and nonirradiated multilayers.

We used x-ray diffraction for an additional characterization of the crystalline quality of the quantum dots in the annealed samples and for the determination of the lattice parameter and size of the crystalline QDs. In Fig. 7 we present the diffraction curves of both nonirradiated and irradiated samples after annealing. We point out that the diffraction curves exhibit more differences than the corresponding

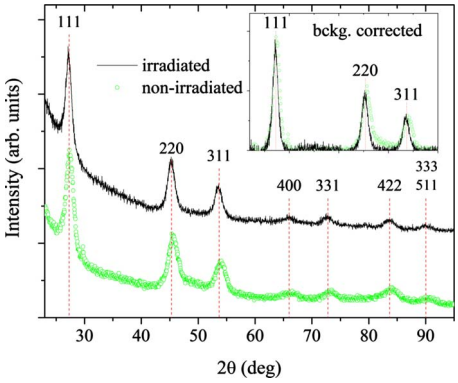

FIG. 7. (Color online) Diffraction curves of the nonirradiated and irradiated multilayers. The inset shows the first three diffraction peaks corrected for background stemming from the substrate scattering.

Raman data shown in Fig. 6(b). The diffraction peaks of the nonirradiated sample are broader and shifted to higher diffraction angles; therefore, this sample contains smaller QDs with smaller lattice parameters. From the positions of the diffraction maxima we determined the lattice parameters of the Ge QDs and we found $0.5605 \pm 8 \times 10^{-4}$ and $0.5657 \pm 8 \times 10^{-4}$ nm, in the nonirradiated and irradiated multilayers, respectively. From the widths of the diffraction peaks we calculated the mean radii of the dots, using the well-known Williamson-Hall procedure[31] and we obtained the values of 3.3 ± 0.2 nm for the nonirradiated and 4.2 ± 0.2 nm for the irradiated multilayers. The obtained values agree well with the GISAXS results shown in Table I.

The difference in the lattice parameters due to the irradiation can be ascribed to the effect of the energy of the interface between the quantum dot and its neighborhood, which is more pronounced for a smaller quantum dot.[32,33] Besides the described differences, the heights of the corresponding diffraction maxima are the same for both curves. Therefore, the irradiation followed by annealing does not cause any significant increase in the concentration of plane defects such as stacking faults and twin planes in the crystalline QDs; these defects would affect the ratios of the heights of the diffraction peaks.[32]

Further, we have used IR absorption spectroscopy to estimate roughly the influence of the irradiation on the quality of the SiO_2 matrix. The IR spectra of the nonirradiated and irradiated multilayers after annealing are displayed in Fig. 8. Both IR spectra are very similar; three peaks characteristic for the amorphous SiO_2 (Refs. 34 and 35) appear at the same positions for both samples. From this position we determined the effective chemical composition of the SiO_x material[34,35] and we found $x = 2.1 \pm 0.2$ in agreement with our assumption of the SiO_2 matrix.

VI. CONCLUSION

We have investigated the influence of ion beam irradiation of $(Ge+SiO_2)/SiO_2$ multilayers on their structural properties, and we have developed a model for the analysis of the GISAXS intensity distributions measured on these multilay-

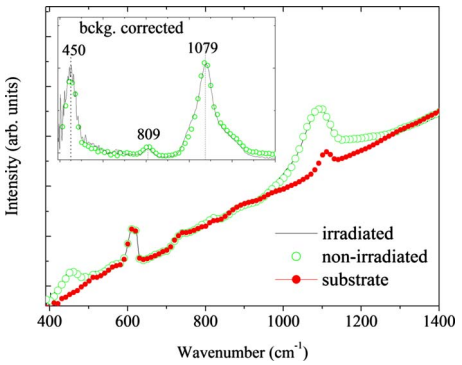

FIG. 8. (Color online) Infrared absorption spectra of the irradiated and nonirradiated samples. The inset shows the difference of the measured curves. The spectra are corrected to the contribution of pure Si substrate.

ers. We have shown that the irradiation process induces a nucleation of quantum dots along the irradiation direction and a formation of regularly ordered QD arrays. The observed process substantially improves the correlation in the positions of the quantum dots, which is practically absent when the irradiation process is not applied. The observed regular ordering is explained and successfully simulated by a simple phenomenological model, based on energy deposition during the ion passage through the material. Another important conclusion is that the irradiation does not affect the good crystalline quality of quantum dots created after the irradiation by annealing. This result indicates the applicability of this relatively simple method for the production of ordered three-dimensional arrays of quantum dots.

ACKNOWLEDGMENTS

The authors are grateful to Medeja Gec for the transmission electron microscopy and Aleksa Pavlešin for assistance in the sample deposition. M.B. acknowledges the support from the National Foundation for Science, Higher Education and Technological Development of the Republic Croatia. M.B. and V.H. acknowledge the support from the Ministry of Education of the Czech Republic (Project. No. MSM 0021620834) as well as from the NAMASTE project (the Framework-Seven EU program), and G.D. acknowledges the support of the Slovenian Research Agency (Grant No. P2-0084).

APPENDIX

Here, we present the details of the structure model used for the simulation of the GISAXS data. The total scattered intensity is a superposition of the contributions of quantum dots and interface roughness. The intensity from the quantum dots is given by

$$I_{QD}(\boldsymbol{q}) = A|t_i t_f|^2 |\delta\varrho|^2 N_{QD} \left\langle \left| \sum_j \Omega^{\mathrm{FT}}(\boldsymbol{q}) e^{-i(\boldsymbol{q}\cdot\mathbf{R}_j)} \right|^2 \right\rangle, \tag{A1}$$

where $\boldsymbol{q}$ is the complex scattering vector inside the substrate (i.e., corrected to refraction and absorption); A is a constant; $t_{i,f}$ are the Fresnel transmission coefficients of the free surface for the primary and emitted waves, respectively; $\delta\varrho$ is the difference in the electron densities of the quantum dots and the surrounding material of the Ge-rich layers; N_{QD} is the number of irradiated quantum dots; and $\Omega^{\mathrm{FT}}(\boldsymbol{q})$ is the Fourier transformation of the shape function $\Omega(\boldsymbol{r})$ of a quantum dot (unity inside the dot volume and zero outside it). The averaging $\langle\ \rangle$ in Eq. (A1) is performed over the random dot sizes and over the dot positions $\mathbf{R}_j$.

After averaging we obtain the following expression for the scattered intensity:

$$I(Q) = \tag{A2}$$

$$A|t_i t_f|^2 |\delta\varrho|^2 N_{QD}[G_0 f_1 + G_V f_2 (G_1 G_2 G_3 - G_4)], \tag{A3}$$

where

$$G_0 = N_x N_y \gamma_L^2 \gamma_3 \frac{1 - (\xi_3 \xi_3^*)^{N_z}}{1 - \xi_3 \xi_3^*},$$

$$G_{1,2} = N_{x,y} + 2\ \mathrm{Re}\left\{ \frac{\xi_{1,2}\eta_L}{\xi_{1,2}\eta_L - 1} \left[\frac{\xi_{1,2}\eta_L - (\xi_{1,2}\eta_L)^{N_{x,y}}}{1 - \xi_{1,2}\eta_L} - N_{x,y} + 1 \right] \right\},$$

$$G_3 = \frac{\xi_3^{N_z} - 1}{\xi_3 - 1} \frac{\xi_3^{*N_z} - 1}{\xi_3^* - 1},$$

$$G_V = \left| e^{-q_\perp^2 (\sigma_{LV}^2/2)} \right|^4 \left| e^{-q_\perp^2 (\sigma_{VV}^2/2) - q_\parallel^2 (\sigma_{VL}^2/2)} \right|^2,$$

$$G_4 = N_x N_y \frac{1 - (\xi_3 \xi_3^*)^{N_z}}{1 - \xi_3 \xi_3^*},$$

$$f_1 = \langle |\Omega^{\mathrm{FT}}(\boldsymbol{q})|^2 \rangle,$$

$$f_2 = |\langle \Omega^{\mathrm{FT}}(\boldsymbol{q}) \rangle|^2, \tag{A4}$$

and

$$\xi_1 = e^{-i\boldsymbol{q}\cdot\boldsymbol{a}_1},$$

$$\xi_2 = e^{-i\boldsymbol{q}\cdot\boldsymbol{a}_2},$$

$$\xi_3 = e^{-i\boldsymbol{q}\cdot\boldsymbol{a}_3}, \tag{A5}$$

$$\eta_L = e^{-q_\parallel^2 (\sigma_{LL}^2/2)},$$

$$\eta_3 = e^{-q_\parallel^2 (\sigma_{VL}^2/2)},$$

$$\gamma_L = e^{2\ \mathrm{Im}(q_\perp)^2 \sigma_{LV}^2},$$

$$\gamma_3 = e^{2\ \mathrm{Im}(q_\perp)^2 \sigma_{VV}^2}.$$

The contribution of the interface roughness to the

scattered intensity is proportional to the square of the contrast in the refraction indices of the SiO_2 and $Ge+SiO_2$ layers, i.e., to the square of the Ge content in the latter layers *between the QDs*. Since this content decreases during the postgrowth annealing, the roughness contribution is significant for nonannealed samples only. For the description of the diffuse scattering from the interface roughness we used a standard fractal approach with oblique vertical replication.[20,36] A detailed numerical comparison of measured and simulated intensity maps made it possible to determine both the parameters of the paracrystal model describing the dot positions and the roughness model.

[1] A. P. Alivisatos, Science **271**, 933 (1996).
[2] A. L. Goodwin, Nat. Nanotechnol. **3**, 710 (2008).
[3] P. Michler, A. Kiraz, C. Becher, W. V. Schoenfeld, P. M. Petroff, Lidong Zhang, E. Hu, and A. Imamolu, Science **290**, 2282 (2000).
[4] Xiaoqin Li, Yanwen Wu, Duncan Steel, D. Gammon, T. H. Stievater, D. S. Katzer, D. Park, C. Piermarocchi, and L. J. Sham, Science **301**, 809 (2003).
[5] http://www.nanotec.org.uk/: Nanoscience and Nanotechnologies: Opportunities and Uncertainties, report of The Royal Society and The Royal Academy of Engineering, London, 2004).
[6] W. C. W. Chan, D. J. Maxwell, X. Gao, R. E. Bailey, M. Han, and S. Nie, Curr. Opin. Biotechnol. **13**, 40 (2002).
[7] A. Courty, A. Mermet, P. A. Alboy, E. Duval, and M. P. Pileni, Nature Mater. **4**, 395 (2005).
[8] M. Buljan, U. V. Desnica, M. Ivanda, N. Radić, P. Dubček, G. Dražić, K. Salamon, S. Bernstorff, and V. Holý, Phys. Rev. B **79**, 035310 (2009).
[9] M. Buljan, U. V. Desnica, G. Dražić, M. Ivanda, N. Radić, P. Dubček, K. Salamon, S. Bernstorff, and V. Holý, Nanotechnology **20**, 085612 (2009).
[10] D. Grützmacher, T. Fromherz, C. Dais, J. Stangl, E. Müller, Y. Ekinci, H. H. Solak, H. Sigg, R. T. Lechner, E. Wintersberger, S. Birner, V. Holý, and G. Bauer, Nano Lett. **7**, 3150 (2007).
[11] A. Konchenko, Y. Nakayama, I. Matsuda, S. Hasegawa, Y. Nakamura, and M. Ichikawa, Phys. Rev. B **73**, 113311 (2006).
[12] Y. Nakayama, I. Matsuda, S. Hasegawa, and M. Ichikawa, Appl. Phys. Lett. **88**, 253102 (2006).
[13] J. K. Shen, X. L. Wu, C. Tan, R. K. Yan, and X. M. Bao, Phys. Lett. A **300**, 307 (2002).
[14] S. K. Ray and K. Das, Opt. Mater. (Amsterdam, Neth.) **27**, 948 (2005).
[15] A. Dowd, R. G. Elliman, M. Samoc, and B. Luther-Davies, Appl. Phys. Lett. **74**, 239 (1999).
[16] Q. Xu, I. D. Sharp, C. W. Yuan, D. O. Yi, C. Y. Liao, A. M. Glaeser, A. M. Minor, J. W. Beeman, M. C. Ridgway, P. Kluth, J. W. Ager, D. C. Chrzan, and E. E. Haller, Phys. Rev. Lett. **97**, 155701 (2006).
[17] A. Kanjilal, J. Lundsgaard Hansen, P. Gaiduk, A. Nylandsted Larsen, N. Cherkashin, A. Claverie, P. Normand, E. Kapelanakis, D. Skarlatos, and D. Tsoukalas, Appl. Phys. Lett. **82**, 1212 (2003).
[18] T. C. Chang, S. T. Yan, P. T. Liu, C. W. Chen, S. H. Lin, and S. M. Sze, Electrochem. Solid-State Lett. **7**, G17 (2004).
[19] M. Buljan, I. Bogdanović-Radović, M. Karlušić, U. V. Desnica, G. Dražić, N. Radić, P. Dubček, K. Salamon, S. Bernstorff, and V. Holý, Appl. Phys. Lett. **95**, 063104 (2009).
[20] U. Pietsch, V. Holý, and T. Baumbach, *High-Resolution X-Ray Scattering* (Springer-Verlag, New York, 2004).
[21] R. Hosemann and S. N. Bagchi, *Direct Analysis of Diffraction by Matter* (North-Holland, Amsterdam, 1962).
[22] K. Salamon, O. Milat, M. Buljan, U. V. Desnica, N. Radić, P. Dubček, and S. Bernstorff, Thin Solid Films **517**, 1899 (2009).
[23] P. I. Gaiduk, A. N. Larsen, C. Trautmann, and M. Toulemonde, Phys. Rev. B **66**, 045316 (2002).
[24] I. Batra, T. Mohanty, and D. Kanjilal, Nucl. Instrum. Methods Phys. Res. B **266**, 3107 (2008).
[25] K. H. Heinig, T. Müller, B. Schmidt, M. Strobel, and W. Möller, Appl. Phys. A: Mater. Sci. Process. **77**, 17 (2003).
[26] M. Schmidbauer, M. Hanke, and R. Kohler, Phys. Rev. B **71**, 115323 (2005).
[27] J. F. Ziegler, Nucl. Instrum. Methods Phys. Res. B **219**, 1027 (2004).
[28] A. Meftah, F. Brisard, J. M. Constantini, E. Dooryhee, M. Hage-Ali, M. Hervieu, J. P. Stoquert, F. Studer, and M. Toulemonde, Phys. Rev. B **49**, 12457 (1994).
[29] T. Fanfoni and M. Tomellini, J. Phys.: Condens. Matter **17**, R571 (2005).
[30] F. S. Ham, J. Phys. Chem. Solids **6**, 335 (1958).
[31] G. K. Williamson and W. Hall, Acta Metall. **1**, 22 (1953).
[32] M. Buljan, U. V. Desnica, N. Radić, G. Dražić, Z. Matěj, V. Valeš, and V. Holý, J. Appl. Crystallogr. **42**, 660 (2009).
[33] B. Palosz, S. Stelmakh, E. Grzanka, S. Gierlotka, and W. Palosz, Z. Kristallogr. **222**, 580 (2007).
[34] D. V. Tsu, G. Lucovsky, and B. N. Davidson, Phys. Rev. B **40**, 1795 (1989).
[35] L. Schumann, A. Lehmann, H. Sobotta, V. Riede, U. Teschner, and K. Hubner, Phys. Status Solidi B **110**, K69 (1982).
[36] V. Holý, J. Stangl, T. Fromherz, R. T. Lechner, E. Wintersberger, G. Bauer, C. Dais, E. Muller, and D. Grutzmacher, Phys. Rev. B **79**, 035324 (2009).